Journal of Asian Earth Sciences 147 (2017) 439–451

Contents lists available at ScienceDirect

Journal of Asian Earth Sciences

journal homepage: www.elsevier.com/locate/jseaes

Full length article

Assessment of maximum earthquake potential of the Kopili fault zone in northeast India and strong ground motion simulation

Anup K. Sutar[a,*], Mithila Verma[a], Ajeet P. Pandey[b], B.K. Bansal[a], P. Rajendra Prasad[c], P. Rama Rao[c], Babita Sharma[b]

[a] Geoscience/Seismology Division, Ministry of Earth Sciences, New Delhi, India
[b] National Center for Seismology, Ministry of Earth Sciences, New Delhi, India
[c] Dept. of Geophysics, Andhra University, Visakhapatnam, India

ARTICLE INFO

Keywords:
Kopili fault zone
Fault slip rate
Strain budget
Maximum magnitude
Strong ground motion simulation
PGA
Seismic hazard

ABSTRACT

Maximum magnitude (MM) earthquake in the Kopili fault zone of North-East India has been assessed using different approaches, which are primarily dependent on various parameters such as fault geometry, slip rate, geodetic moment rate, and convergence rate. The analyses reveal that the source zone has accumulated strain energy, during the last 72 years since 1943, enough to produce a strong earthquake of magnitude ≥ 7. On supplementing with the historical data, we conclude M_w7.3 as the maximum potential earthquake for the Kopili source zone. Such large earthquake, on its occurrence, may cause widespread significant ground shakings and damage to infrastructures in the study region. We, therefore, also simulated strong ground motion, in the form of peak ground acceleration (PGA), for the M_w7.3 potential earthquake using Empirical Green's Function (EGF) approach for ten different sites. In the analysis, an earthquake of magnitude M_w6.5, which has been simulated using a recorded M_w5.3 earthquake, is used as Green's Function. The two-step approach is adopted in the simulation process, as the required criteria, i.e., moment ratio of < 1000 between the target potential event (M_w7.3) and the element event (M_w5.3) could not be met. We found that the cities like Tezpur, Masamari, Tumuki, Dhekiajuli, Nagaon, Bomdila, Udalguri, Seppa, Hajoi, Behali, Guwahati, and Itanagar that are located ~ 60–130 km from the source zone may experience very strong to moderate ground shaking with PGA ranging between 0.36–0.14 g. However, the cities located in the distance range of ~ 130 – 300 km from the source, namely Jorhat, Ziro, Mokokchung, Dhubri, and Kokrajhar are expected to have low ground shaking with PGA < 0.14 g. The study therefore provides valuable insights to the likely seismic hazard scenario in north-east India.

1. Introduction

The North-East India is located in close proximal to the Indo-Burmese arc, one of the most seismically active regions of the country, has witnessed two great historical earthquakes of magnitude M ≥ 8 in last 150 years, viz., M8.1 the Great Shillong earthquake of 1897 and M8.5 the Great Assam earthquake of 1950. Nevertheless, many moderate to large earthquakes have been occurring quite often for centuries and have shattered the region. The collision between the Indian and Eurasian plates in the north and the subduction of the Indian plate underneath the Burmese arc in the east characterize the region as a triple junction (Hazarika et al., 2011) and provide a favourable tectonic framework for intense seismic activity in the region. The seismicity in the entire northeast region, however, may not be explained by the subduction vis-à-vis collisional tectonic regimes. Instead, the role of intervening faults has often been hypothesized for generating widespread seismicity in the region; for example, the 1897 Shillong earthquake (M8.1), the 1869 Cachar earthquake (M7.5) and the 1943 Hajoi earthquake (M7.3) are few important events associated with such intervening faults (Bilham and England, 2001; Kayal, 2008). Initially the 1897 Shillong earthquake was considered to be a result of the collision between the Indian and Eurasian plates; however, it was later attributed to the activation of the Oldham fault (Bilham and England, 2001).

The NW-SE trending Kopili fault, which transects in the middle of the northeastern state of Assam separating the Shillong plateau and its sub-massif the Mikir Hills Plateau (Fig. 1), is widely considered to be the causative source for the 1869 M7.5 Cachar and the 1943 M7.3 Hajoi earthquakes (Dasgupta et al., 2000; Nandy, 2001; Kayal et al., 2012). Kayal et al. (2010) analyzed a number of significant strong earthquakes in the region, including 1941 M6.5 Tezpur and 2001 M6.9 Bhutan

* Corresponding author.
E-mail address: anupseismo@gmail.com (A.K. Sutar).

http://dx.doi.org/10.1016/j.jseaes.2017.07.035
Received 10 October 2016; Received in revised form 7 July 2017; Accepted 18 July 2017
Available online 20 July 2017

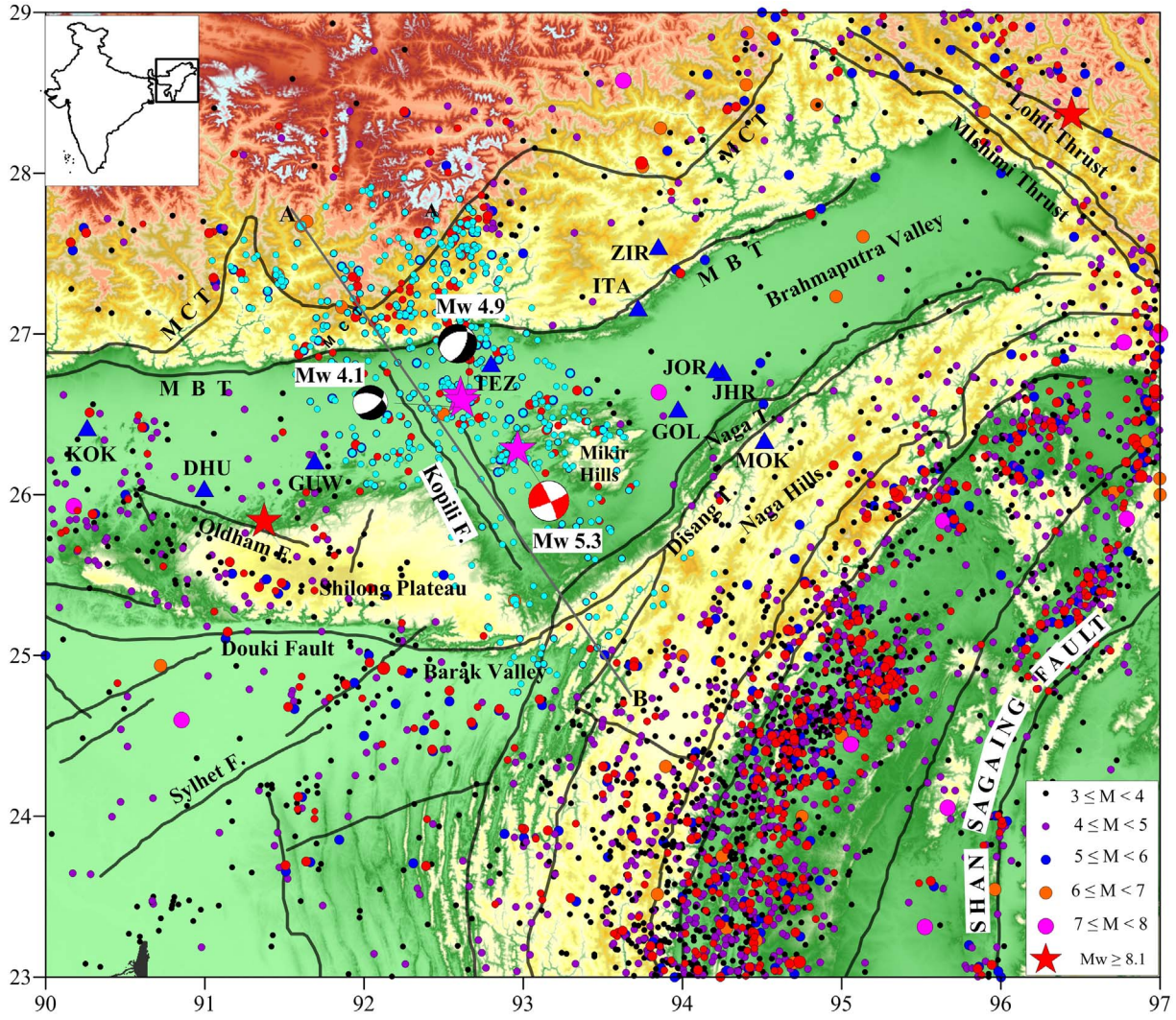

Fig. 1. Major tectonic elements of northeast India and its adjoining region are displayed over a topographic map. The abbreviated labels are MBT (main boundary thrust), MCT (main central thrust), F (fault), and T (thrust). Violet stars represent the recent events that have been used in the analyses. The epicenter of the 1897 (M 8.1) and 1950 (M 8.5) historical earthquakes are shown as red star. Blue triangles represent the seismic stations in the study area and are annotated with respective station code; details of which are given in Table 6. Closed circles with increasing size depict epicenter of earthquakes with magnitude ranging $3 < M < 8$. Cyan circles represent $M > 3$ events, which were used in estimation of the slip rate of the Kopili fault. Red circles indicate the EHB relocated events. Black straight line represents profile AB coinciding with the NW-SE trending Kopili fault. (For interpretation of the references to colour in this figure legend, the reader is referred to the web version of this article.)

earthquakes, and attributed their causative source to the Kopili fault. Large historical earthquakes ($M > 7$) in the Kopili fault zone, which have caused devastation in the northeastern India and also affected the seismogenic behavior of the fault in the recent past, characterize the Kopili fault active. However, there is no large event in the Kopili fault zone since the 1943 M7.3 Hajoi earthquake. In the present study, we have made an attempt for the first time to assess the maximum magnitude (MM) earthquake in the Kopili fault zone using different approaches primarily dependent on the fault geometry, slip rate, geodetic moment rate, and convergence rate. We have also generated the seismic hazard scenario in the study region due to the M_w7.3 maximum potential earthquake in the Kopili fault zone. A three step approach has been adopted in the study, viz., i) estimation of maximum potential earthquake of Kopili fault using available geological and geophysical inputs, ii) estimation of strain accumulation using GPS data as well as release of seismic energy in the form of small events occurred after 1943 M7.3 Hajoi earthquake, and iii) simulation of hazard scenario in the form of Peak Ground Acceleration (PGA) using Empirical Green's Function (EGF) technique. In the analysis, an intermediate step was introduced to generate the ground motion for M_w6.5 earthquake using an observed M_w5.3 earthquake. The M_w6.5 event was then used as an element event for simulating strong ground motion for the M_w7.3 maximum potential earthquake. We also validated the EGF technique using the two observed events of M_w4.9 and M_w4.1 from the Kopili fault zone.

2. Geology and tectonics

The Kopili fault source zone in North-East India is about 300 km long and 50 km wide surrounding the Kopili lineament (Nandy, 1980). The fault is named after the Kopili River, one of the southern tributaries of the Brahmaputra River, originating from the Borail range of the North Cachar Hills and flowing across Karbianglong, Nagaon, and Morigaon districts of Assam (Fig. 1). A number of buried faults and lineaments including, Kopili had been identified using remote sensing technique (Nandy and Dasgupta, 1986). Later, the Kopili lineament was confirmed as an active fault on the basis of its intense seismic activity (Nandy, 2001). This lineament cuts through three major tectonic regimes of the region, namely, (i) the eastern Himalayan mountain range, (ii) Arakan Yoma subduction zone, and (iii) the lower Assam valley.

The northern part of the Kopili fault extends deep into the eastern Himalayan mountain range that rise abruptly from the Brahmaputra

plains and merge to the Tibetan plateau further north (Fig. 1). The entire Himalayan range has been characterized into Sub, Lesser and Higher Himalaya from south to north. Each of these blocks is bounded by intra-continental thrusts, such as the Frontal Foot Hill Thrust (FHT) between Brahmaputra plains and Sub-Himalaya Siwalik, Main Boundary Thrust (MBT) separating Sub Himalaya from the Lesser Himalaya, and the Main Central Thrust (MCT) between the Lesser and Higher Himalaya. Many studies have further shown evidences that confirm the extension of the Kopili fault even beyond the MBT and MCT (Nandy and Dasgupta, 1986; Nandy, 2001; Kayal et al., 2010). NW-SE trending Mishmi hills, to the east of the Kopili fault, have been considered as northward continuation of the Myanmar hills of Burma and they constitute a major portion of the Himalayan Syntaxis. The Mishmi hills tectonic block has been further traversed by NW-SE trending thrust/reverse faults such as Mishmi thrust and Lohit thrust (Thakur and Jain, 1975). The Kopili fault in the south is assumed to cut across the Naga-Disang thrust of Arakan Yoma Subduction Zone (Fig. 1) that consists of the Indo-Myanmar ranges (Arakan Yoma, Chin Hills and Naga Hills), the Myanmar basin (Central low lands) and the eastern highlands of Shan Plateau (Bender, 1983).

The Shillong plateau in the west of the Kopili fault is considered to be separated from the peninsular India and has moved to the east by 300 km along the Dauki fault (Evans, 1964). This plateau is an east-west trending oblong horst block with a raised platform uplifted about 600 m to 1800 m above the Bangladesh plains (Bilham and England, 2001) and is also etched with closely spaced liners. The smooth light toned surface of the Shillong plateau is characterized with crisscross orienting rectilinear drainage patterns. These patterns show a spectacular feature revealing extraordinary straight courses of rivers and streams along the prominent lineaments, which are surface expressions of joints and faults. Such geologic attributes and stratigraphy have been also found in the Mikir Hills massif and considered as an eastern extension of the Shillong plateau. These two geologically similar blocks, i.e., the Mikir Hills massif and the Shillong plateau are separated by the NW-SE trending seismically active tectonic belt along the Kopili fault (Fig. 1).

3. Source zone characterization

The source zone characterization of a fault provides various input parameters required for the estimation of maximum earthquake potential of the fault. We have carried out the source characterization of the Kopili fault and constrained the fault geometry to ascertain its length and width on the basis of observational seismological data and the results of tomography reported by Bhattacharya et al. (2008). They found a prominent NW–SE trending low V_p structure in between the Shillong Plateau and the Mikir Hills. The position and orientation of such low V_p feature are consistent with the Kopili fault in the region. Fig. 2 illustrates V_p tomograms for the study area at different depths, viz., 10 km, 20 km, 30 km and 40 km. The velocity image at 10 km depth does not show linear feature, suggesting non-existence of the Kopili fault at that depth. Low V_p linear zone is evident in both the 20 km and 30 km depths windows, which we have ascribed to deep-seated Kopili fault. Geologically mapped 300–400 km long Kopili lineament on the ground surface would probably be the surface expression of the deep seated structure.

The observed low V_p structure orienting NW-SE at 20–30 km depth is found terminated in the 40 km depth window, and a prominent high V_p structure imaged underneath. Such high velocity structure at deeper horizon has been contended to be the stress concentrator, causing high seismic activity in the region. In the present study, we analyzed velocity tomogram at 20 km depth using digital image processing and inferred the length of the Kopili fault as 240 km (Fig. 2).

The down-dip end of the Kopili fault has been characterized using two different approaches (Phan et al., 2012), i) on the basis of seismic characteristics of the fault, and ii) considering the change in mechanical characteristics with depth. Nazareth and Hauksson (2004) have estimated the lower end of a seismogenic fault using depth distribution of background seismicity. Many researchers have found this approach effective in estimating the down-dip end of the fault and further envisaged that larger magnitude earthquakes tend to nucleate at the base of the seismogenic fault (Lay and Wallace, 1995; Bhattacharya et al., 2008; Mishra and Zhao, 2003). Moreover, the thickness of the brittle layer in the Earth's crust is assumed as fault width (Scholz, 1990). In this study, we have used EHB (Engdahl et al., 1998) relocated events from International Seismological Centre (ISC) Bulletin (http://www.isc.ac.uk, International Seismological Centre, United Kingdom, 2009) within an area of 400 × 300 sq km covering the Kopili fault zone. All the seismic events were projected on NW-SE trending profile AB, as depicted in Fig. 1, and a depth distribution plot of these events is obtained along the profile (Fig. 3). We mention that the profile AB is restricted in the SE to exclude the effect of subducting Indian plate beneath the Burmese arc. However, the NW end of the profile covers a section of the Himalaya, as the Kopili fault extends beyond the MCT and MBT. Fig. 3 clearly depicts the influence of tectonics in the outer Himalaya, which is apparent in the NW part of the depth profile. Focal depths of the earthquakes in this part lie in the depth range of 5 – 20 km, which are similar to other events reported along the Himalayan arc. The seismicity in between the MBT and the Naga Thrust is predominantly confined to ~ 30–50 km depth range. In a recent study, Bhattacharya et al. (2008) have found depth extension of the Kopili fault system in the range of 20–40 km. Eventually, we inferred the seismogenic thickness of the Kopili fault as 20 km, which has been approximated to the width of the fault (Kocharyan et al., 2011) in the analysis.

Other critical parameters used in the analysis, viz., strike and dip of the Kopili fault and the fault motion were derived using the focal mechanism of the seismic events and GPS velocity vector respectively. Fig. 4 shows beach balls representing fault plane solutions of the earthquakes in the study region during the period (1964–2012); relevant data are taken from different sources (Nandy and Dasgupta, 1991; Kayal et al., 2012) including, online URL www.globalcmt.org. It is evident from the plot that the fault plane solutions are mainly of strike-slip nature, except a few that shows normal and thrust types with small strike-slip component. The dextral nature of the Kopili fault is inferred from fault plane solutions of the recorded earthquakes (Nandy and Dasgupta, 1991; Kayal et al., 2012). Further, the dextral motion along the Kopili fault has also been confirmed from the GPS studies (Mahesh et al., 2012; Barman et al., 2016).

It is apparent from the beach ball plot that most of the earthquakes having thrust mechanism with strike-slip component are located close to the northern flank of the Kopili fault, which is assumed to extend beyond the MBT and MCT. The normal fault planes with strike-slip component and the planes having pure strike slip motions are mainly distributed in the middle part of the Kopili fault. The fault plane solutions with strike slip motion characterizing the behavior of the Kopili fault have been segregated to obtain strike and dip of the Kopili fault (Fig. 5). The distribution of strike values is found in the range 257–355°, while the dip values show significant variation in the range 66–86°. In the analysis, we inferred representative average strike and dip values of the Kopili fault as 311° and 77° respectively.

4. Estimation of maximum magnitude (MM) earthquake

The maximum magnitude earthquake is considered essential for seismic hazard assessment of any region, which may be estimated by different methodologies. In the present study, we have estimated the MM on the basis of empirical relations, fault slip rate, GPS derived strain rate and slip budget as described in the following sections.

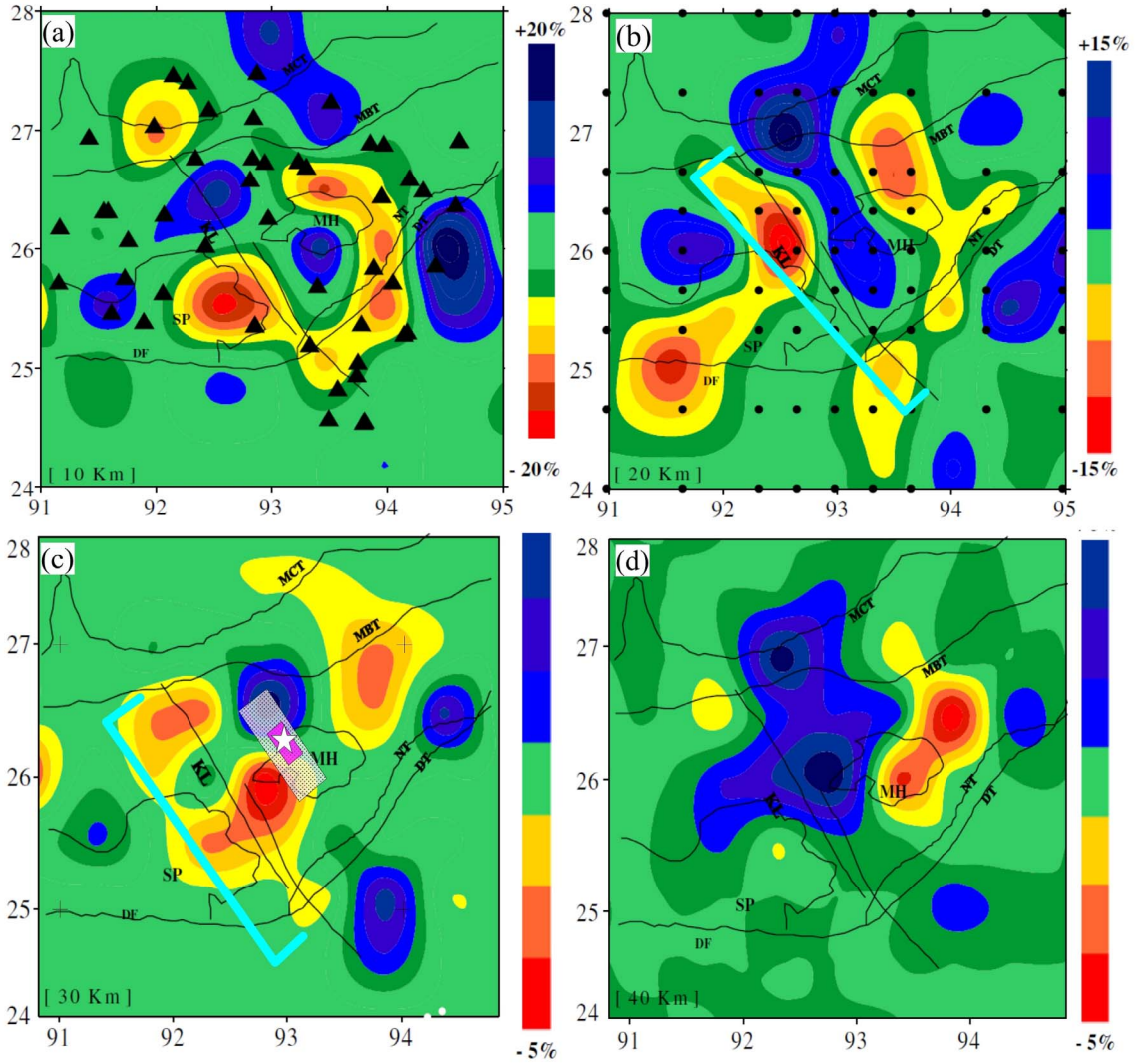

Fig. 2. V_p tomograms at different depths, viz., 10 km, 20 km, 30 km and 40 km in the study area (after Bhattacharya et al., 2008). Low velocity linear feature along the Kopili lineament is clearly depicted in the depth panels of 20 km (b) and 30 km (c); however, the same is absent in the depth panels of 10 km (a) and 40 km (d). Thick cyan line represents the length of the Kopili fault used in the analysis. Solid triangles, as shown in the panel (a), demonstrate the location of seismic stations. Tectonic features are shown as thin black lines labeled with abbreviations KL (Kopili lineament), SP (Shilong Plateau), DF (Douki fault), MH (Mikir hills), NT (Naga thrust) and DT (Disang thrust); the remaining abbreviations are detailed in the caption of the Fig. 1. White star in the panel (c) represents the epicenter of the M_w5.3 earthquake. Two concentric rectangles, white and pink shaded regions, show hypothetical rupture zones of the simulated target events M_w7.3 and M_w6.5, respectively. (For interpretation of the references to colour in this figure legend, the reader is referred to the web version of this article.)

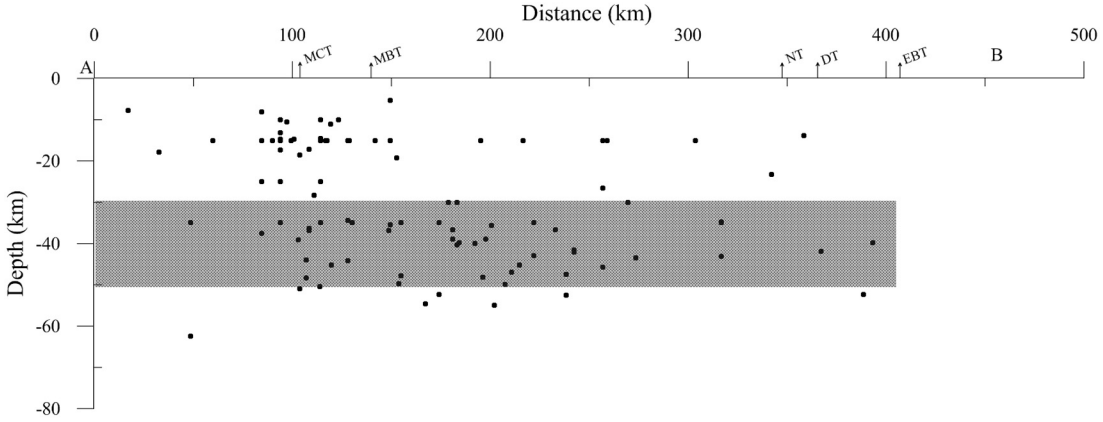

Fig. 3. Depth plot of EHB (Engdahl et al., 1998) relocated events along the profile AB. The intersections between the major tectonic units and the profile are shown with up facing arrow. Label EBT represents the eastern boundary thrust zone; the remaining abbreviations are detailed in the captions of the Figs. 1 and 2.

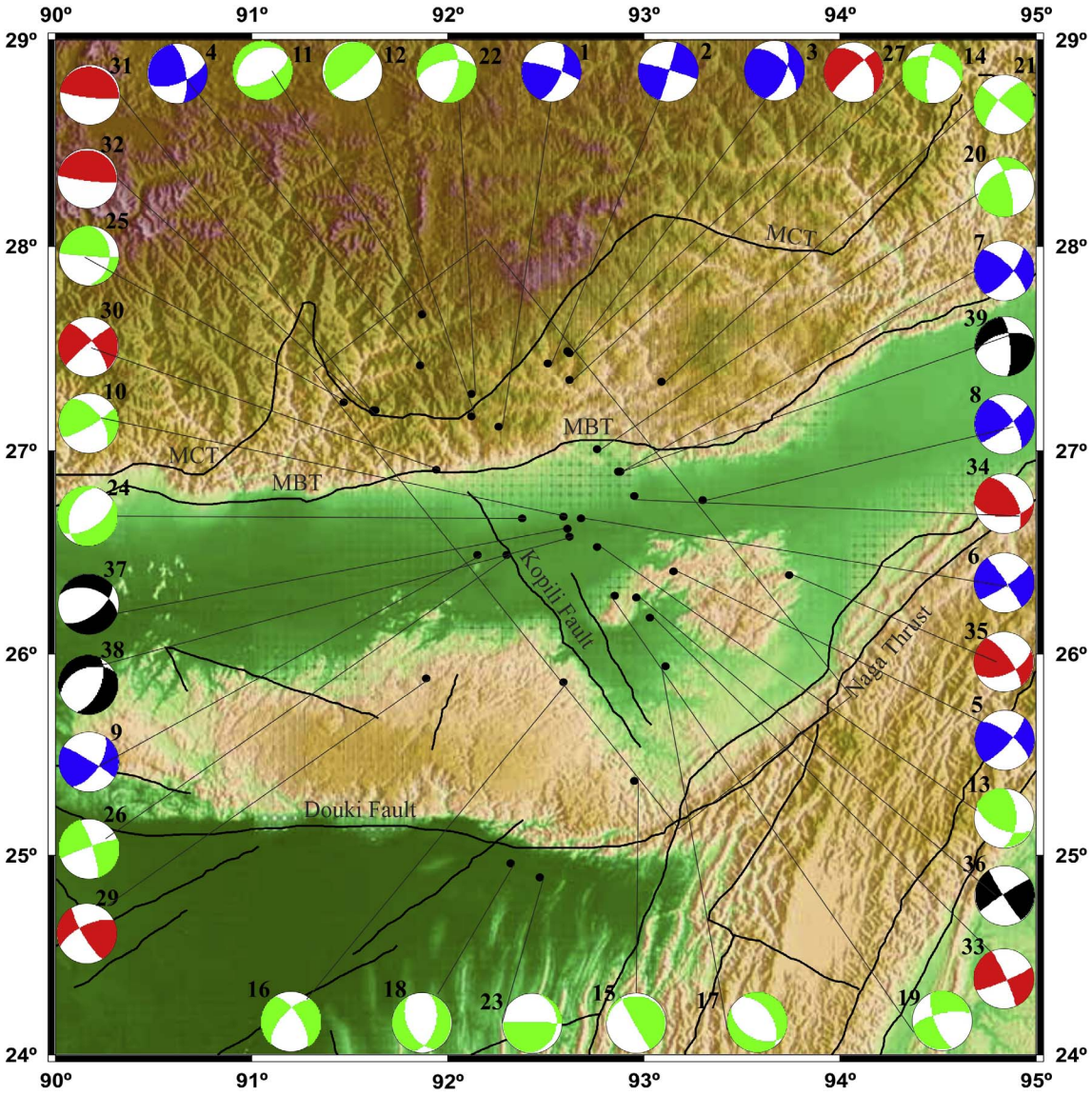

Fig. 4. Beach balls plot showing the fault plane solutions of earthquakes (M 3.6 – 6.3) near the Kopili fault zone for the period 1964–2012. The data of fault plane solutions used in blue, green and red beach balls are taken from Nandy (2001), Kayal et al. (2012) and online URL www.globalcmt.org respectively. Black beach balls are plotted from the present study. (For interpretation of the references to colour in this figure legend, the reader is referred to the web version of this article.)

4.1. Estimation of MM using empirical relations

Estimation of maximum magnitude (MM) earthquake on a fault using various empirical relations (Wyss, 1979; Wells and Coppersmith, 1994; Somerville et al., 1999; WGCEP, 2003; Hanks and Bakun, 2002; Papazachos et al., 2004) is well accepted, globally. In this study, six different empirical equations (Table 1) have been used to estimate the MM, which are dependent on parameters of the fault geometry such as length, width, and area of the fault. The length, width, and area of the Kopili fault have been already ascertained as 240 km, 20 km, and 4800 sq km respectively in the previous section. These estimates were used in the empirical relations (Table 1) to obtain the MM of the Kopili fault zone. The results are consistent and the average MM of the Kopili fault source zone is found to be M_w7.7.

4.2. Estimation of MM using fault slip rate

The slip rate for the Kopili fault has been estimated following the formulation by Bilham and Ambraseys (2005). Cumulative seismic moment release (Table 2) from 553 earthquakes (M > 3), for the period (1943–2015), has been used in the analysis and a slip rate 0.868 mm/yr is obtained for the Kopili fault. The GPS studies in the north-eastern India, however, reveal different slip rates, viz., 2.62 ± 0.79 mm/yr (Barman et al., 2016) and 3.0 ± 1.5 mm/yr (Mahesh et al., 2012), and also show right lateral slip velocity. Consequently, we analyzed maximum magnitude (MM) of the Kopili fault for three different slip rates, i.e., 3 mm/yr, 2 mm/yr and 0.868 mm/yr, using the equations listed in Table 3. It is found that MM of the Kopili fault varies in the range 7.1–7.9 with an average of M_w7.5.

4.3. Estimation of MM using GPS derived strain rate

One of the most stable estimates of geodetic strain rate can be obtained using the relation (Oncel and Wilson, 2006):

$$\in'_{max} = \max(abs(\lambda 1), \mathrm{abs}(\lambda 2)) \quad (1)$$

where $\in'_{max}$ is defined as maximum geodetic strain rate and is estimated as the larger absolute value of λ1 or λ2, i.e., the most extensional or compressional Eigen values of the strain rate tensor. In this study, the principal components of strain rates (λ1 and λ2) have been adopted

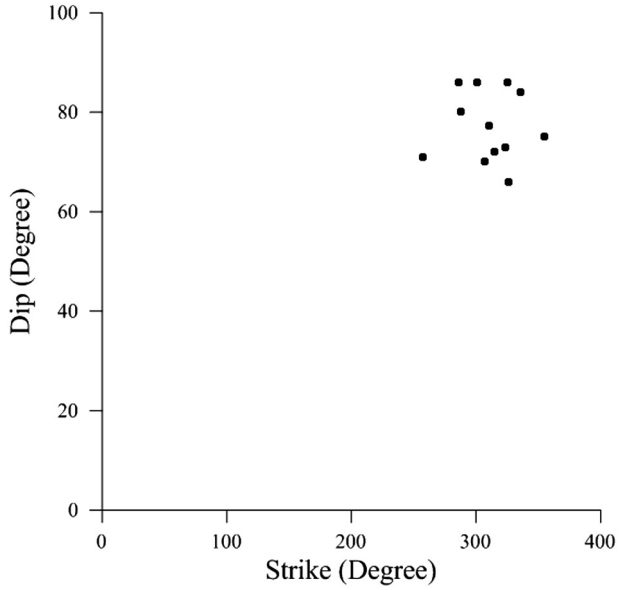

Fig. 5. Plot showing strike and dip distribution of the events with epicenters near the Kopili fault zone.

Table 2
Estimated slip rate in the Kopili fault zone using cumulative moment release.

Seismic moment (NM)	Fault length (m)	Fault width (m)	Rigidity (μ) (N/m^2)	Time (in yr)	Slip rate (m/yr)
9.90E+22	2.40E+05	2.00E+04	3.3×10^{10}	72	8.68E−04

Table 3
Estimated maximum magnitude (MM) earthquake using fault slip rates.

Slip rate (mm/yr)	Formula	Maximum magnitude (MM)	Remarks
3	M_w = 5.12 + 1.16Log (L) − 0.2Log(S)	7.7	Anderson et al. (1996)
2	M_w = 5.12 + 1.16Log (L) − 0.2Log(S)	7.8	
0.868	M_w = 5.12 + 1.16Log (L) − 0.2Log(S)	7.9	
3	M_s = 7.223 + 1.265Log(S)	7.8	WCC (1979)
2	M_s = 7.223 + 1.265Log(S)	7.6	
0.868	M_s = 7.223 + 1.265Log(S)	7.1	

S: Fault slip rate, L: Length of the fault

from Reddy et al. (2012). Assuming that the net strain rate is equal to the maximum strain rate, the geodetic moment rate ($M_{geodetic}$) has been obtained using the relation (Kostrov, 1974):

$$M_{geodetic} = 2\mu A H_s \epsilon'_{max} \quad (2)$$

Where, μ is the shear rigidity, H_s is the thickness of the seismogenic zone and A is the surface area over which strain is distributed.

Shear rigidity for the study area is assumed as 3.3×10^{10} N/m^2 (Bilham and Ambraseys, 2005) in the analysis. We estimated the maximum magnitude (MM) of the Kopili fault using geodetic moment rate (Table 4), which is found to be 6.42 E + 18 Nm. However, assuming a constant geodetic moment rate, the accumulated seismic moment along the Kopili fault source zone is obtained as 4.62 E + 20 Nm in the inter-seismic period of 72 years. The inter-seismic period has been considered as the time since the last M7.3 event occurred in 1943 till date. For this period, we have also computed the cumulative seismic moment release due to M > 3 earthquakes as 9.9×10^{18} Nm. Consequently, using the left over strain energy, it is inferred that the Kopili fault is capable of producing an earthquake of M_w7.1.(See. Table 4)

4.4. Estimation of MM using the slip budget estimate

We analyzed the fraction of accumulated strain owing to the plate convergence that released through seismic slip process. It was assumed that the accumulation of the elastic strain along the Kopili fault is continued at the plate convergence rate and later the strain energy gets released in the form of earthquakes. Considering the steady rate of the plate convergence at 0.016–0.022 m/yr (Mukul et al., 2010), in 72 years of the inter-seismic period the cumulative slip increased to 1.156–1.584 m and the net current slip budget raised to ~ 1.2 m. We also infer that ~ 0.5 m slip has been consumed until now along the Kopili fault zone since the time evolution of seismicity (Fig. 6). All events M ≥ 4.0 including, pre-shocks, swarms and aftershocks were considered in the analysis, in addition to the main shocks, presuming that these events would be contributing to the cumulative displacement. The analysis based on the relation between the magnitude and surface displacement (Wells and Coppersmith, 1994) suggests the available slip deficit to be in the range 0.656 m - 1.084 m, which is sufficient to generate an earthquake of magnitude ~ M_w7.0 (Table 5).

5. Strong ground motion simulations in the study region

We have computed MM earthquake associated with the Kopili fault of north-east India using different approaches and found it to be M ≥ 7. Although the empirical relations used in the analyses are mainly developed utilizing the global data sets, they yet provide consistent result. Further, the seismicity analysis in and around the Kopili source zone using earthquake data of last 100 years reveals that the zone has witnessed one large earthquake of magnitude M7.3 in the year 1943. In view of this and also considering the possibility of repeating a similar earthquake on Kopili fault, we assess M_w7.3 as the maximum potential earthquake for the Kopili fault zone.

The strong ground motion simulation for the potential event of M_w7.3 has been carried out for ten sites in the study region using Empirical Green's Function (EGF) technique (Irikura et al., 1997; Miyake et al., 1999; Sharma et al., 2013). This technique precisely

Table 1
Maximum magnitude (MM) earthquake of the Kopili fault zone using different empirical relations.

Sl. No.	Length (km)	Width (km)	Area (sq km)	Formula	Maximum magnitude (MM)	Standard deviation	Remarks
1	240	20	4800	M = 4/3Log (A) + 3.07	7.9	σ = 0.12	Hanks and Bakun (2002)
2	240	20	4800	Log(L) = 0.59 M − 2.30	7.9	σ = 0.14	Papazachos et al. (2004)
4	240	20	4800	Log(W) = 0.23 M − 0.49	7.8		Papazachos et al. (2004)
5	240	20	4800	M = log(A) + 4.15	7.8		Wyss (1979)
6	240	20	4800	M = 1.02Log(A) + 3.98	7.7	σ = 0.23	Wells and Coppersmith (1994)
7	240	20	4800	M = log(A) + 4.2	7.9	σ = 0.12	WGCEP (2003)
8	240	20	4800	M = log(A) + 3.95	7.6		Somerville et al. (1999)

M: Magnitude of the event, A: Area of the fault, L: Length of the fault, W: Width of the fault

Table 4
Estimated maximum magnitude (MM) earthquake using geodetic moment rate.

Far field velocity (m/yr)	Seismological locking depth (m)	Strain release rate (NM/yr)	Geodetic moment rate (NM/yr)	Accumulated moment (NM) in 72 yrs period	Moment released (NM)	Maximum magnitude, M_w
2.8397E-2	2.00E + 04	4.46E − 07	6.42E + 18	4.62E + 20	9.90E + 18	7.1

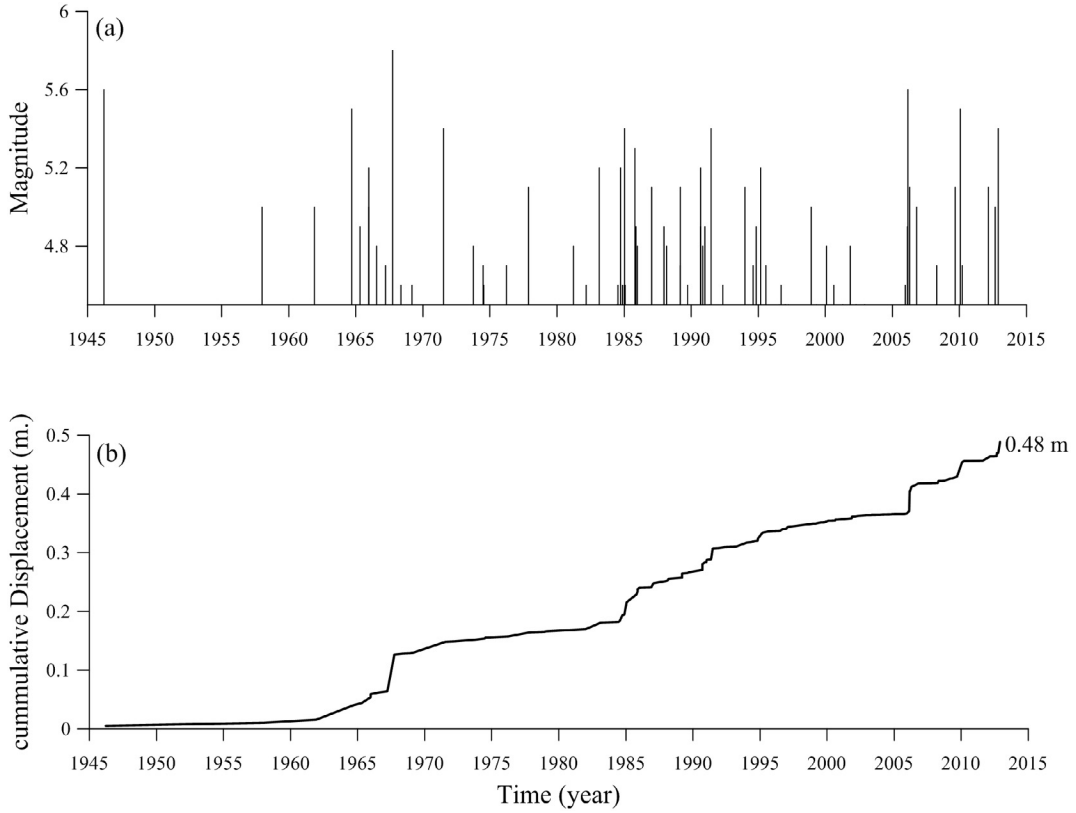

Fig. 6. (a) Plot showing time evolution of seismicity along the Kopili fault (source: www.isc.ac.uk). (b) Plot showing time evolution of cumulative displacements in the Kopili fault zone.

Table 5
Estimated maximum magnitude (MM) earthquake using convergence rate.

Convergence rate (m/yr)	Accumulated slip (m)	Cumulative displacement (m)	Slip deficit (m)	Maximum magnitude, M_w	Formula (Wells and Coppersmith, 1994)
0.016–0.022	1.156–1.584	0.5	0.656–1.084	6.8–7.0	$M_w = 6.93 + 0.82\log(D)$

Table 6
Details of seismic stations including site class and geological attributes.

Station name	Code	Latitude	Longitude	Site class	Site specific geological attributes
Tezpur	TEZ	26.79	92.79	B	Alluvium
Itanagar	ITA	27.14	93.72	B	Sandstones
Molkochung	MOK	26.32	94.51	B	Sandstones
Ziro	ZIR	27.52	93.85	B	Quartzite/schist/gneiss
Jorhat[#]	JHR	26.75	94.20	C	Alluvium
Jorhat[#]	JOR	26.74	94.25	C	Alluvium
Dhubri	DHU	26.02	90.00	C	Alluvium
Golaghat	GOL	26.51	93.97	B	Sandstones
Guwhati	GUW	26.19	91.75	C	Alluvium
Khokrajhar	KOK	26.40	90.26	C	Soils (slope washed)

[#] Stations JHR and JOR at Jorhat are maintained by IIT Roorkee and IMD New Delhi respectively.

simulate the ground motion for an unknown large magnitude event (i.e. target event), using a recorded lower magnitude earthquake (i.e. element event) on the same seismic source. Nevertheless, this technique has a limitation of simulating strong ground motions at specific sites where the recordings are available for a smaller magnitude element event.

The M_w5.3 earthquake of 11 May 2012 that had occurred on the Kopili fault, located in the Nagaon district of Assam state (Fig. 1), was taken as element event in the analysis. This earthquake was recorded using accelerometers at 10 different sites in the study region (Table 6). Before simulating the strong ground motion for the target earthquake M_w7.3, we validated the EGF technique using two earthquakes from the same seismic source; also they were recorded at the same seismic station. The two moderate earthquakes, viz., M_w4.1 and M_w4.9 occurred on the Kopili fault on 19 August 2012, both with normal faulting mechanism (Fig. 1). These events were well recorded at Tezpur station that was operating in the study region. The fault plane solutions of these two earthquakes were obtained using the procedure adopted from (Verma et al., 2015) and the results are shown in Fig. 1. The stress drop, corner frequency and source radius were also estimated using Brune's model (Brune, 1970; Chopra et al., 2014). Details of hypocentral as well as source parameters of these events and that of the element earthquake

Table 7
Estimated source parameters of M_w5.3, 4.9 and 4.1 earthquakes.

Sl. No	Time		Latitude (°N)	Longitude (°E)	Depth (km)	Magnitude (M_w)	Source parameters		
	dd/mm/yy	hr:mm:ss					Stress drop (bar)	Corner frequency (Hz)	Source radius (km)
1	5/11/2012	12:41:35.5	26.28	92.96	34	5.3	103	0.48	2.7
2	8/19/2012	09:24:49.7	26.62	92.61	38	4.9	95	1.62	1.2
3	8/19/2012	19:04:57.1	26.58	92.62	36	4.1	52	2.59	0.6

Table 8
Parameters used in the simulation of target events (M_w7.3, 6.5 and 4.9) using Empirical Green's Function (EGF) technique.

Magnitude (M_w)	Rupture area (km^2)	Rupture length (km)	Rupture width (km)	Rise time (sec)	Rupture velocity (km/sec)	Area of asperity# (km^2)	Length of asperity# (km)
7.3	1778.3	90.36	19.67	6.56	2.80	363.99	19.07
6.5	338.84	28.84	11.74	2.09	2.80	–	–
4.9	12.30	2.93	4.18	0.21	2.80	–	–

Area and length of Asperity are not considered in case of events with magnitude $M_w < 7$.

Table 9
Three component peak ground acceleration (PGA) values obtained at Tezpur site for recorded and simulated events.

Recorded/simulated events	PGA on longitudinal component (gal)	PGA on transverse component (gal)	PGA on vertical component (gal)	Maximum PGA (gal)
Recorded M_w4.1	8.9	11.2	9.9	11.2
Recorded M_w4.9	16.6	26.3	17.3	26.3
Simulated M_w4.9	24.1	28.2	24.6	28.2

(M_w5.3) are shown in Table 7.

As the epicentres of the M_w4.1 and M_w4.9 earthquakes are found close to each other, the respective propagation paths from the source to the recording station have been assumed to be the same. Also, the focal mechanisms of these two events indicate normal faulting. These criteria eventually provide an ideal condition for carrying out validation of the EGF technique, considering M_w4.9 earthquake as target event and relatively smaller M_w4.1 earthquake as an element event. Table 8 lists the parameters used in simulation of the target event M_w4.9. We simulated the strong ground motion in the form of horizontal peak ground acceleration (PGA) at the site(s), where the element event was recorded. The analysis reveals that the simulated PGA at Tezpur site (i.e. 28.2 gal), for the M_w4.9 event, is ~ 93% in agreement with that of the recorded PGA (i.e. 26.3 gal) at the same site (Table 9). The simulated and recorded accelerograms at the Tezpur station for the M_w4.9 event are shown in Fig. 7a and b. The small deviation in simulated PGA for each component could be attributed to the statistical fluctuations. The recorded accelerogram of the element event M_w4.1, at the Tezpur station, is also shown in Fig. 7c. In addition, Fourier spectra of the recorded and simulated acceleration time history of the M_w4.9 event computed for three components (Fig. 7d) show a satisfactory agreement in the frequency band of 1–20 Hz. Consequent to the successful validation, the EGF technique was applied to simulate ground motions in the form of PGA for potential earthquake (M_w7.3) of the Kopili zone using well recorded lower magnitude element earthquake.

In the simulation, we have considered a two-step approach as direct simulation of the target event M_w7.3 using an observed smaller magnitude event M_w5.3 did not meet the required criteria of moment ratio < 1000 (Irikura et al., 1997; Miyake et al., 1999; Joyner and Boore, 1988; Sharma et al., 2013). First, an intermediate target event (M_w6.5) was simulated taking M_w5.3 as element event in the analysis and consequently, the event M_w6.5 was considered as element event for simulating strong ground motion for the maximum potential earthquake M_w7.3. This technique allowed us to simulate strong ground motion at ten recording sites for two different target events; the intermediate event M_w6.5 and the maximum potential earthquake M_w7.3 of the Kopili fault. The EGF technique requires estimating fault parameters, namely, rise time, rupture velocity and size of the asperity (Table 8) for both the intermediate and the main target events. Asperity, which plays a critical role in strong ground motion simulation, was considered only for M_w7.3 following Somerville et al. (1999). The fault parameters like rupture area, length and width have been estimated following the method described by Wells and Coppersmith (1994), and the area of asperity has been obtained using the formulation of Somerville et al. (1999). The rise time and the rupture velocity of the fault slip have been, however, estimated using the method described by Geller (1976).

While simulating the intermediate target event M_w6.5, we assume the rupture zone and the rupture initiation point at the hypocentral location of the element event M_w5.3, which coincides with the centre of the fault (Fig. 2). Radial propagation of the wave is also considered in the analysis and the simulation has been carried out for three components of the accelerogram. The stress drop ratio which is a sensitive parameter in the analysis was assigned a value of 0.8 as most of the earthquakes in the Himalayan region show constant stress drop with stress drop ratio close to 1 (Sharma et al., 2013). Table 8 lists all relevant parameters that have been used in simulation of ground motion. The recorded accelerograms of the element event M_w5.3 as well as the simulated accelerograms of the target events (M_w6.5 and 7.3) at ten different stations, namely, Tezpur, Golghat, Itanagar, Guwahati, Jorhat (IIT), Jorhat, Ziro, Mokokchung, Dhubri, and Kokrajhar, are shown in Fig. 8. We also analyzed the accelerograms of the element and the target events for the site specific PGA at the ten recording sites spread out across the study region and the results are given in Table 10.

Fig. 9 shows a contour map of simulated PGA in the study region for the maximum potential earthquake M_w7.3 on Kopili fault zone. It is evident that the maximum PGA is 360 gal (i.e. 0.36 g) near Tezpur city, which is located ~ 60 km away from the source; unlike the cases where maximum PGA is observed close to the epicentre. Unfortunately, there was no recording station operating close to the epicenter of the element event M_w5.3 (Fig. 1); hence the PGA near the source could not be simulated within a distance < 60 km. The cities within a radius ~ 30 km from the Tezpur station, namely, Masamari, Tumuki, Dhekiajuli, Rupa and Bomdila, which may experience PGA ranging between 0.27 g and 0.35 g, are kept under very high hazard category. Other cities such as Udalguri, Seppa, Nagaon, Hajoi and Behali etc.,

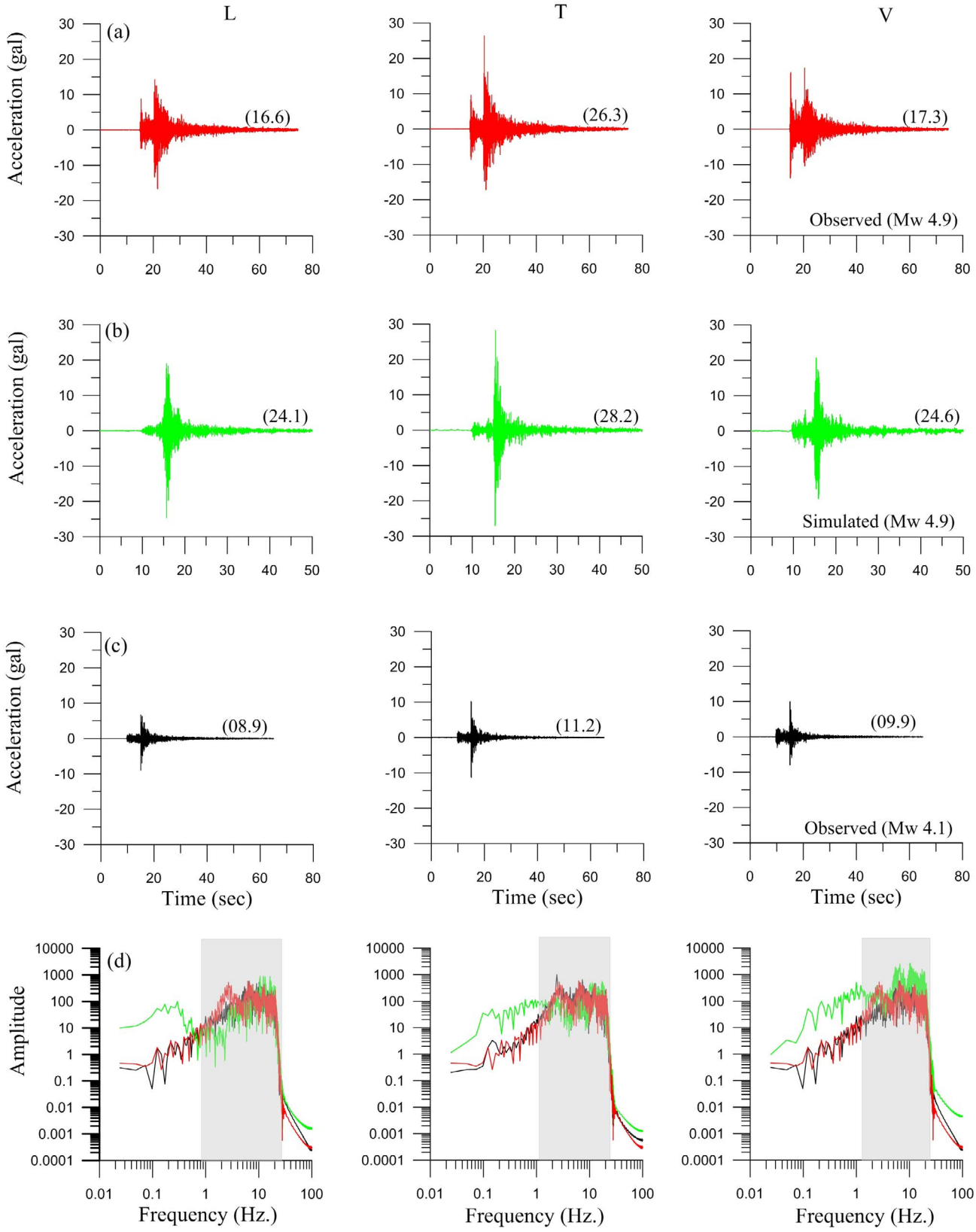

Fig. 7. Plot showing three components acceleration time history of a) observed M_w4.9 event, (b) simulated M_w4.9 event, and (c) observed M_w4.1 event. Panel (d) illustrates the Fourier spectra of acceleration time history of these events for each component. Grey strip represents the frequency band in which the simulated and recorded spectra match well. Labels L, T and V on the top panels represent Longitudinal, Transverse and Vertical components respectively.

expected to experience PGA in the range 0.22–0.26 g, are grouped under high hazard. The cities close to Guwahati, namely, Tamulpur, Nalbari, Rangia, Shillong and those located to the east of Hajoi, namely, Maja, Diphu, etc. may experience moderate hazard in the PGA range of 0.14–0.21 g. However, the remaining cities in the area like Dergaon, Golaghat, Itanagar, Jorhat, Dhubri, Kokrajhar, Golpara, Mokokchung,

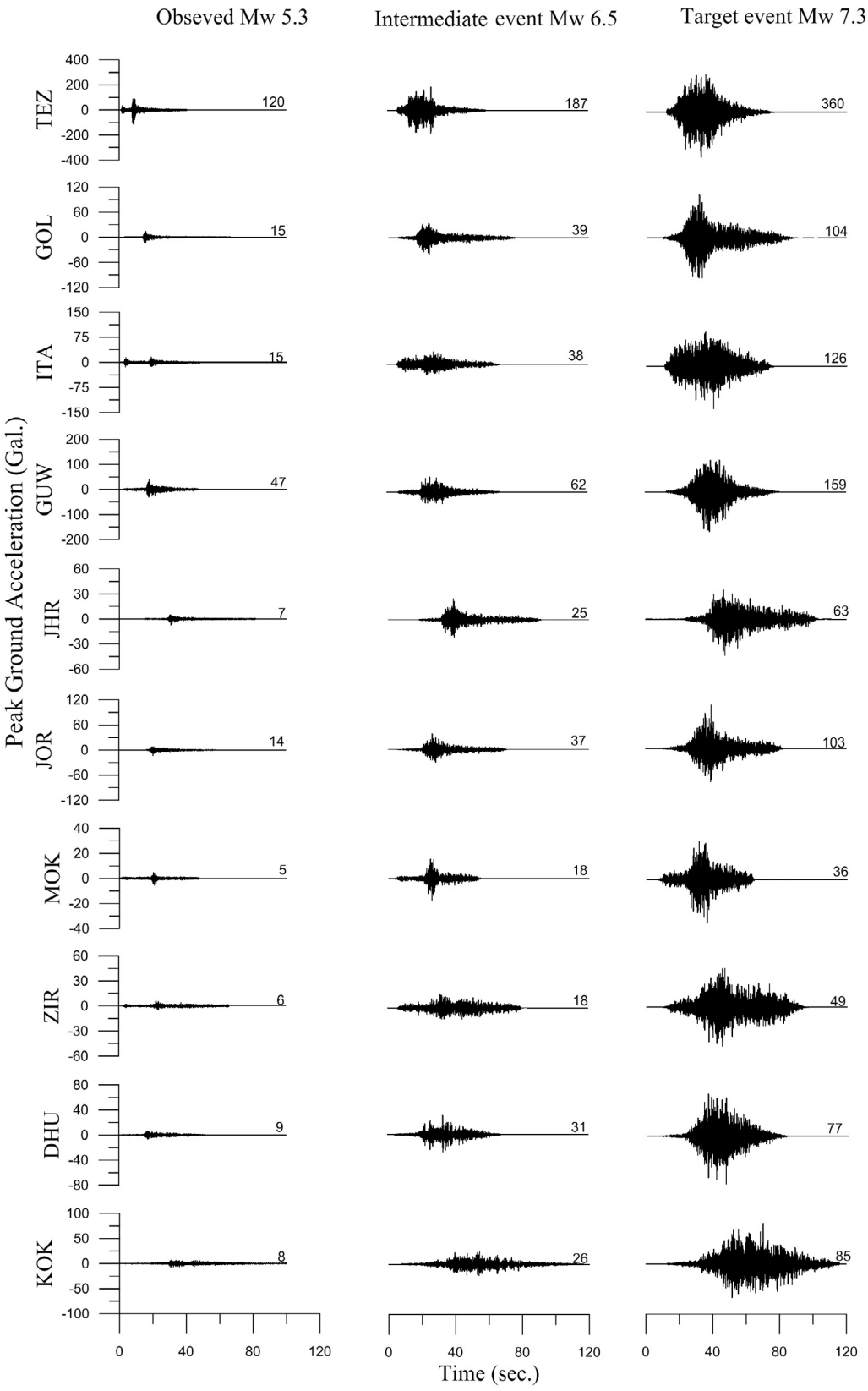

Fig. 8. Acceleration time history showing peak ground acceleration (PGA) at ten seismic stations in the study region for (a) recorded M_w5.3 event, (b) simulated M_w6.5 intermediate event, and (c) simulated M_w7.3 maximum potential event. PGA values (in Gal) are labeled at the end of the traces.

Wokha, North Lakhimpur and Ziro located ~ 130–300 km away from the Kopili fault are placed in low hazard zone with expected PGA < 0.14 g.

The recorded and simulated peak ground accelerations (PGA) have been compared with that of the ground motions estimated through existing attenuation relations for the study area (Fig. 10). We observe from the plot that the PGA (recorded and simulated) values are compatible with attenuation curves, particularly, for the distances ≥ 100 km. However, the attenuation curves as shown in the plots were developed for the hard rock region, whereas the simulated

Table 10
Estimated maximum PGA values at ten sites for the maximum potential earthquake (M_w7.3) and intermediate event (M_w6.5). Observed maximum PGA values for a recorded earthquake (M_w5.3) are also listed for the respective sites.

Station Name	Station code	Epicentral distance* (km)	PGA for M_w 5.3 (gal/g)	PGA for M_w 6.5 (gal/g)	PGA for M_w7.3 (gal/g)
Tezpur	TEZ	60	120/0.122	187/0.191	360/0.367
Golaghat	GOL	104	15/0.015	39/0.040	104/0.106
Itanagar	ITA	122	15/0.015	38/0.039	126/0.129
Guwahati	GUW	127	47/0.048	62/0.063	159/0.162
Jorhat#	JHR	135	7/0.007	25/0.026	63/0.064
Jorhat#	JOR	138	14/0.014	37/0.038	103/0.105
Mokokchung	MOK	155	5/0.005	18/0.018	36/0.037
Ziro	ZIR	164	6/0.006	18/0.018	49/0.050
Dhubri	DHU	198	9/0.009	31/0.032	77/0.079
Kokrajhar	KOK	269	8/0.008	26/0.027	85/0.087

* Epicentral distance mentioned against each station remains constant for all the three events (M_w 5.3, 6.5 and 7.3), as the locations of each event have been opted same in the analyses.

Data from two seismic stations located at Jorhat has been used in the analyses. Stations JHR and JOR are maintained by IIT Roorkee and IMD New Delhi respectively.

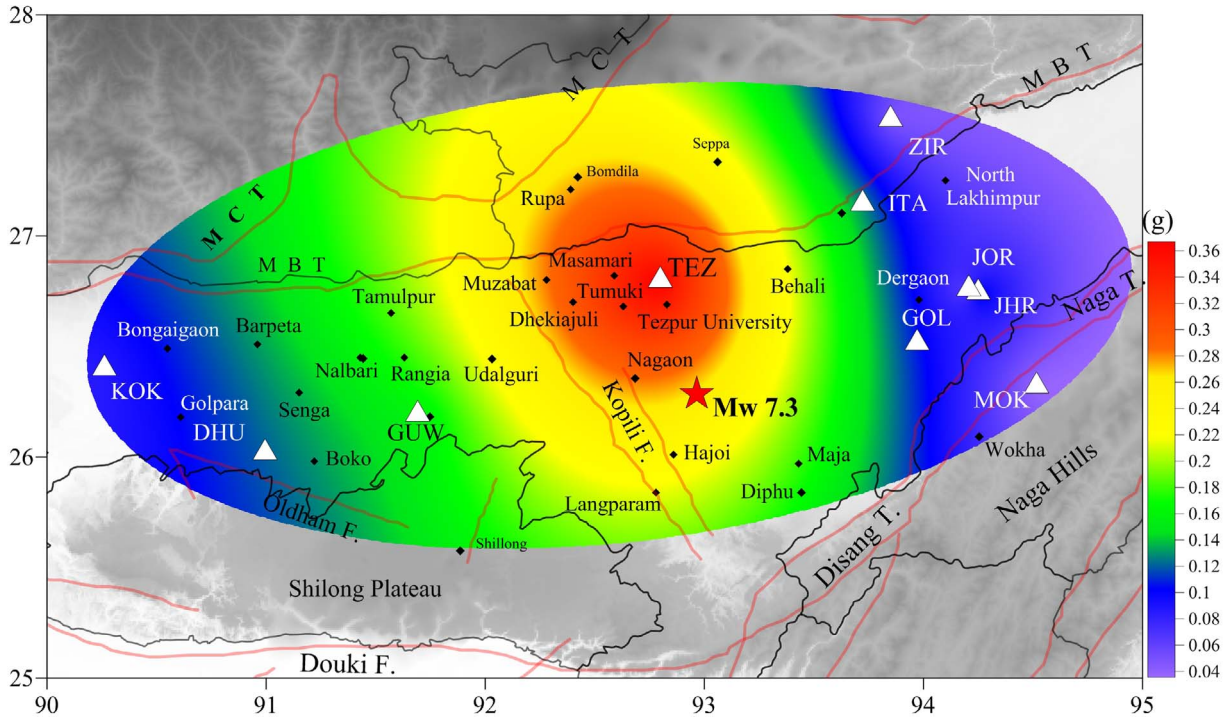

Fig. 9. Colour contour map showing the simulated PGA for the maximum potential earthquake (M_w7.3) of the Kopili fault zone superimposed over local tectonics of the study area. White triangles depict the location of seismic stations. Red star represents the location of the potential earthquake, which is used in the analysis. Important cities in the study region are shown as black diamonds. (For interpretation of the references to colour in this figure legend, the reader is referred to the web version of this article.)

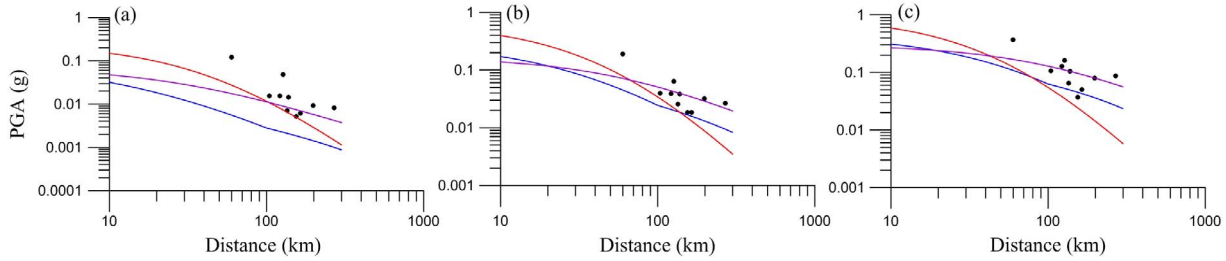

Fig. 10. Variation in PGA at different sites, with increasing distance from the source, are plotted over the attenuation curves of the region for (a) recorded M_w5.3 event, (b) simulated M_w6.5 intermediate event, and (c) simulated M_w7.3 maximum potential event. Three attenuation curves (Iyengar et al., 2010; Sharma et al., 2009 and Nath et al., 2009) are plotted in purple, red and blue, respectively. (For interpretation of the references to colour in this figure legend, the reader is referred to the web version of this article.)

PGA values for ten different sites are obtained on the ground surface that includes the local soil affects.

6. Discussion

In a tectonic regime, seismic sources have different potential of generating large earthquakes and may cause huge loss of lives and severe damage to buildings and infrastructural facilities. We have carried out a detailed analysis to assess the maximum earthquake potential of the Kopili fault zone in north-east India using different approaches, primarily dependent on the fault geometry, slip rate, geodetic moment rate and convergence rate. The estimated MM using different empirical relationships fall in the range M_w7.1 to 7.9. The GPS strain measurement and slip budget analyses, however, suggest MM in relatively lower range M_w7.0 to 7.1. The statistical mean of the estimated MM values using different techniques is M_w7.5. However, this may not truly represent the study region as the empirical relations used in the analysis were developed based on the global data sets. Hence considering the possibility of repeating a large earthquake similar to the one that had occurred on the Kopili fault in 1943, we have assessed M_w7.3 as the maximum potential earthquake of the Kopili fault zone.

We further simulated strong ground motion in the study region at ten different sites, for the potential earthquake M_w7.3, using EGF technique. The site specific strong ground motion has been found to be critical in an earthquake affected region, besides the magnitude of the event itself, which illustrates substantial influence on the damage pattern of buildings and structures. It is evident from the amplitude of earthquake records that the ground motion varies depending on i) the soil cover beneath the observation site, and ii) the topographical location of the site. The peak ground acceleration (PGA) is an important measure of strong ground motion at the site that we can directly record using an operating accelerometer. However, in case there is no functional accelerometer in the region, the site specific ground motions for large earthquakes can be simulated effectively using the EGF technique, provided a smaller magnitude earthquake on the same source is already recorded at the sites. This technique also has an advantage of accommodating the soil effects at the sites while simulating strong ground motions. In this study, we have considered M_w5.3 as an element event (a smaller magnitude recorded earthquake). However, it must be mentioned that the simulation of a large magnitude target event M_w7.3 directly from the element event M_w5.3 was not found feasible; hence a two-step approach was adopted. The Tezpur station was the nearest site at about 60 km away from the source, which showed maximum PGA 360 gal (i.e. 0.36 g) for the potential event M_w7.3 (Fig. 9). It is also evident from the analysis that the ground motion at Tezpur site is significantly large with PGA 187 gal (i.e. 0.19 g) for the intermediate event M_w6.5 (Table 10). The element event M_w5.3 was not recorded in the vicinity of the source; hence we could not simulate PGA at sites within a distance $<$ 60 km from the source.

The perceived strong ground shaking in case of the potential as well as intermediate earthquakes may cause extensive damage in and around the Tezpur city. BIS (2002) has attributed the zone factors 0.10 g, 0.16 g, 0.24 g, and 0.36 g in ascending seismic hazard levels for the country, which classify four different zones from low hazard to very high hazard through moderate and high hazard zones. The cities in north-east India, namely, Masamari, Tumuki, Dhekiajuli, Nagaon, Bomdila, Udalguri, Seppa, Hajoi, Behali, Guwahati and Itanagar, which are located in the distance range of 60–130 km from the Kopili source, may experience very strong to moderate ground shaking with PGA ranging between 0.35 g and 0.14 g for M_w7.3 maximum potential earthquake. However, the cities located at distances ~ 130–300 km, namely, Jorhat, Ziro, Mokokchung, Dhubri, and Kokrajhar are expected to show low ground shaking with PGA $<$ 0.14 g.

We also found that the Guwahati, Itanagar, and Golaghat sites, though located equidistant from the Kopili source, show substantial variation in recorded and simulated PGA. The variation in PGA suggests that the distance to the fault is not the only consideration for ground motion, rather the directional effect (Stein and Wysession, 2003) and the local site effect (Verma et al., 2014; Verma and Bansal, 2013) may also play a critical role. Guwahati city is situated on an alluvial plain, whereas the Golaghat and Itanagar cities are located on sandstone formation (Mittal et al., 2012). We have also observed a significant change in PGA at two nearby located seismic stations (JHR and JOR), which were operating in Jorhat city over different geological attributes. The JOR site has higher PGA as it is located close to the Brahmaputra river bed underlain by soft alluvial deposits, while the JHR site, which recorded lower PGA, is situated over harder strata. Verma et al. (2014) have shown the role of soft sediments, particularly, the alluvial deposits, which influence the damage pattern significantly.

7. Conclusions

We have analyzed various seismic parameters to constrain the critical geometrical attributes of the Kopili fault zone, namely length, width and area of the fault. These attributes together with slip rate, convergence rate and geodetic moment rate have been used in empirical relations, to assess the maximum magnitude (MM) potential earthquake for the Kopili fault source zone. The results suggest that the source zone has accumulated sufficient strain energy to generate a strong earthquake of magnitude $\geq$ 7. In this study, we have assessed an earthquake with magnitude M_w7.3 as the maximum potential earthquake of the Kopili fault source zone and carried out the corresponding site specific ground motion simulation using EGF technique. An earthquake of magnitude M_w5.3, recorded at different sites, is used as an element event in the simulation. The study indicates that the sites located in the distance range ~ 60–130 km from the Kopili source zone may experience high PGA (0.36–0.14 g); Tezpur being the closest site is expected to have highest PGA (i.e. 0.36 g). The sites located beyond 130 km from the source may experience low PGA ($<$ 0.14 g). The strong ground motion scenario as generated for the study region will be useful for land use planning, development of infrastructures and retrofitting of the existing buildings.

Acknowledgement

The authors acknowledge with thanks to the Secretary, Ministry of Earth Sciences for his continued support and encouragement. We also thank Dr. B. R. Arora and Dr. S. Roy for their valuable comments that improved the manuscript. Strong motion data provided by India Meteorological Department (IMD), New Delhi and Indian Institute of Technology (IIT), Roorkee, without which this work would have not accomplished, are profusely acknowledged. The online data from www.isc.ac.uk and www.globalcmt.org were found useful in completing the work successfully. An earlier version of the manuscript has benefited from reviews by anonymous reviewers, to whom we are grateful. Mei-Fu Zhou and the anonymous reviewers, whose comments helped in improving the quality of the current manuscript significantly, are sincerely acknowledged.

References

Anderson, J.G., Wesnousky, S.G., Stirling, M.W., 1996. Earthquake size as a function of fault slip rate. Bull. Seismol. Soc. Am. 86, 683–690.

Barman, P., Ray, J.D., Kumar, A., Chowdhury, J.D., Mahanta, K., 2016. Estimation of present-day inter-seismic deformation in Kopili fault zone of northeast India using GPS measurements. Geomatics, Nat. Hazards and Risk 72, 586–599. http://dx.doi.org/10.1080/19475705.2014.983187.

Bender, F., 1983. Geology of Burma. Beitrage zur Regionalen Geologie der Erde, Borntraeger, Stuttgart, Band 16, 10.

Bhattacharya, P.M., Mukhopadhyay, S., Majumdar, R.K., Kayal, J.R., 2008. 3-D seismic structure of the northeast India region and its implications for local and regional tectonics. J. Asian Earth Sci. 33, 25–41.

Bilham, R., England, P., 2001. Plateau pop-up in the 1897 Assam earthquake. Nature 410, 806–809.

Bilham, R., Ambraseys, N., 2005. Apparent Himalayan slip deficit from the summation of

seismic moments for Himalayan earthquakes, 1500–2000. Curr. Sci. 88, 1658–1663.
BIS, 2002. Indian standard criteria for earthquake resistant design of structure. Part 1 resistant provision and buildings. Bureau of Indian Standards, New Delhi.
Brune, J.N., 1970. Tectonic stress and the spectra of seismic shear waves from earthquakes. Geophys. Res. Lett. 75, 4997–5009.
Chopra, S., Sharma, J., Sutar, A., Bansal, B.K., 2014. Estimation of source parameters of M_w6.9 Sikkim earthquake and modeling of ground motions to determine causative fault. Pure Appl. Geophys. 171, 1311–1328. http://dx.doi.org/10.1007/s00024-013-0722-6.
Dasgupta, S., et al., 2000. Seismotectonic atlas of india and its environs. Geological Survey of India, Kolkata.
Engdahl, E.R., Van delHi lat, R., Buland, R., 1998. Global teleseismic earthquake relocation with improved travel times and procedures for depth determination. Bull. Seismol. Soc. Am. 88, 722–743.
Evans, P., 1964. Tectonic framework of Assam. J. Geol. Soc. India 5, 80–96.
Geller, R.S., 1976. Body force equivalents for stress drop seismic sources. Bull. Seismol. Soc. Am. 66, 1801–1804.
Hanks, T.C., Bakun, W.H., 2002. A bilinear source-scaling model for M-logA observations of continental earthquakes. Bull. Seismol. Soc. Am. 92, 1841–1846.
Hazarika, D., Arora, B.R., Bora, C., 2011. Crustal structure in the northeast India-Asia collision zone: constraints from receiver function analysis. Geophys. J. Int. 188, 737–749.
Irikura, K., Kagawa, T., Sekiguchi, H., 1997. Revision of the empirical Green's function method. Program and Abstracts of the Seismological Society of Japan 2, B25.
Iyengar, R.N., et al., 2010. Development of probabilistic seismic hazard map of India. Technical Report National Disaster Management Authority, New Delhi.
Joyner, W.B., Boore, D.M., 1988. Measurement, Characterization, and prediction of strong ground motion. In: Earthquake engineering and soil dynamics II-recent advances in ground motion evaluation, geotechnical special publication, New York, 20, pp. 43–102.
Kayal, J.R., 2008. Microearthquake seismology and seismotectonics of South Asia. Springer publication, New York.
Kayal, J.R., Arefiev, S.S., Baruah, S., Tatevossian, R., Gogoi, N., Sanoujam, M., Gautam, J.L., Hazarika, D., Borah, D., 2010. The 2009 Bhutan and Assam felt earthquakes (M_w6.3 and 5.1) at the Kopili fault in the northeast Himalaya region. Geomatics, Natural Hazards and Risk 1, 273–281.
Kayal, J.R., Arefiev, S.S., Baruah, S., Hazarika, D., Gogoi, N., Gautam, J.L., Baruah, S., Dorbath, C., Tatevossian, R., 2012. Large and great earthquakes in the Shillong plateau–Assam valley area of Northeast India region: Pop-up and transverse tectonics. Tectonophysics 532–535, 186–192.
Kocharyan, G.G., Kishkina, S.B., Ostapchuk, A.A., 2011. Seismogenic width of a fault zone. Dokl. Earth Sci. 437, 412–415. http://dx.doi.org/10.1134/S1028334X11030147.
Kostrov, B.V., 1974. Seismic moment and energy of earthquakes and seismic flow of rock. Izvestiya, Phys. Solid Earth 1, 23–40.
Lay, T., Wallace, T.C., 1995. Modern global seismology. USA Academic Press, New York, pp. 521.
Mahesh, P., Catherine, J.K., Gahalaut, V.K., Kundu, B., Ambikapathy, A., Bansal, A., Premkishore, L., Narsaiah, M., Ghavri, S., Chadha, R.K., Choudhary, P., Singh, D.K., Singh, S.K., Kumar, S., Nagarajan, B., Bhatt, B.C., Tiwari, R.P., Kumar, A., Kumar, A., Harsh, B., Kalita, S., 2012. Rigid Indian plate: constraints from GPS measurements. Gondwana Res. 22, 1068–1072.
Mishra, O.P., Zhao, D., 2003. Crack density, saturation rate and porosity at the 2001 Bhuj, India, earthquake hypocenter: a fluid driven earthquake? Earth Planet. Sci. Lett. 212, 393–405.
Mittal, H., Kumar, A., Ramhmachhuani, R., 2012. Indian National strong motion instrumentation network and site characterization of its stations. Int. J. Geosci. 3, 1151–1167.
Miyake, H., Iwata, T., Irikura, K., 1999. Strong ground motion simulation and source modeling of the Kagoshima-ken Hokuseibu earthquakes of March 26 (M_{JMA} 6.5) and May 13 (M_{JMA} 6.3), 1997 using empirical Green's Function method. J. Seismol. Soc. Japan 51, 431–442.
Mukul, M., Jade, S., Bhattacharya, A.K., Bhusan, K., 2010. Crustal shortening in convergent orogens: insights from Global Positioning System (GPS) measurements in Northeast India. J. Geol. Soc. India 75, 302–312.
Nandy, D.R., 1980. Tectonic patterns in northeastern India. Indian J. Earth Sci. 7, 103–107.
Nandy, D.R., Dasgupta, S., 1986. Application of remote sensing in regional geological studies, a case study in northeastern part of India. In: Proceedings of the international seminar on photogrammetry and remote sensing for developing countries, T.4/P6.1-T.4-P/6.4.
Nandy, D.R., Dasgupta, S., 1991. Seismotectonic domains of northeastern India and adjacent areas. Phys. Chem. Earth 18, 371–384.
Nandy, D.R., 2001. Geodynamics of Northeastern India and the adjoining region. ACB Publication, Kolkata.
Nath, S.K., Raj, A., Thingbaijam, K.K.S., Kumar, A., 2009. Ground motion synthesis and seismic scenario in Guwahati city- A stochastic approach. Seismol. Res. Lett. 80, 233–2421.
Nazareth, J.J., Hauksson, E., 2004. The seismogenic thickness of the southern California crust. Bull. Seismol. Soc. Am. 94, 940–960.
Oncel, A.O., Wilson, T., 2006. Evaluation of earthquake potential along the Northern Anatolian Fault Zone in the Marmara Sea using comparisons of GPS strain and seismotectonic parameters. Tectonophysics 418, 205–218.
Papazachos, B.C., Scordilis, E.M., Panagiotopoulos, D.G., Papazachos, C.B., Karakaisis, G.F., 2004. Global relations between seismic fault parameters and moment magnitude of earthquakes. Bull. Geol. Soc. Greece 36, 1482–1489.
Phan, Trong.Trinh., Ngo, Van.Liem., Nguyen, Van.Huong., Hoang, Quang.Vinh., Bui, Van.Thom., Bui, Thi.Thao., Mai, Thanh.Tan., Nguyen, Hoang., 2012. Late quaternary tectonics and seismotectonics along the Red River fault zone, North Vietnam. Earth Sci. Rev. 114, 224–235.
Reddy, C.D., Sunil, P.S., Prajapati, S.K., Ponraj, M., Amrithraj, S., 2012. Geodynamics of the Ne Indian lithosphere: geodetic and seismotectonic perspective. Memoir of the Geol. Soc. India 77, 241–250 ISBN: 978-81-907636-2-2.
Scholz, C.H., 1990. The mechanics of earthquakes and faulting. Cambridge University Press, New York, pp. 439.
Sharma, M.L., Douglas, J., Bungum, H., Kotadia, J., 2009. Ground motion prediction equations based on data from the Himalayan and Zagros regions. J. Earthquake Eng. 13, 1191–1210.
Sharma, B., Chopra, S., Sutar, A.K., Bansal, B.K., 2013. Estimation of strong ground motion from a great earthquake M_w8.5 in central seismic gap region, Himalaya (India) using empirical Green's function technique. Pure Appl. Geophys. 170, 2127–2138.
Somerville, P.G., Irikura, K., Graves, R., Sawada, S., Wald, D., Abrahamson, N., Iwasaki, Y., Kagawa, T., Smith, N., Kowada, A., 1999. Characterizing earthquake slip models for the prediction of strong ground motion. Seismol. Res. Lett. 70, 59–80.
Stein, S., Wysession, M., 2003. An Introduction to Seismology, Earthquakes and Earth Structure. Blackwell Publishing Ltd., U.K.
Thakur, V.C., Jain, A.K., 1975. Some observation on deformation metamorphism and tectonic significance of the rocks of some parts of the Mishmi Hills, Lohit District (NEFA) Arunachal Pradesh. Himalayan Geol. 5, 339–364.
Verma, M., Bansal, B.K., 2013. Seismic hazard assessment and mitigation in India: an overview. Int. J. Earth Sci. 102, 1203–1218.
Verma, M., Singh, R.J., Bansal, B.K., 2014. Soft sediments and damage pattern: a few case studies from large Indian earthquakes vis-a-vis seismic risk evaluation. Nat. Hazards 74, 1829–1851. http://dx.doi.org/10.1007/s11069-014-1283-4.
Verma, M., Sutar, A.K., Bansal, B.K., Arora, B.R., Bhat, G.M., 2015. M_W 4.9 earthquake of 21 August, 2014 in Kangra region, Northwest Himalaya: Seismotectonics implications. J. Asian Earth Sci. 109, 29–37.
Wells, D.L., Coppersmith, K.J., 1994. New empirical relationships among magnitude, rupture length, rupture width, rupture area, and surface displacement. Bull. Seismol. Soc. Am. 84, 974–1002.
WGCEP (Working Group on California Earthquake Probabilities), 2003. Earthquake probabilities in the San Francisco Bay region, 2002–2031. Open File Report, U.S. Geological Survey, 03–214.
WCC, 1979. Report of the evaluation of maximum earthquake and site ground motion parameters associated with the offshore zone of deformation, San Onofre Nuclear Generating station. Report to Southern California Edison Company, Woodward-Clyde Consultants, San Francisco.
Wyss, M., 1979. Estimating maximum expectable magnitude of earthquakes from fault dimensions. Geology 7, 336–340.